

A Possible Extension of the Scutum-Centaurus Arm into the Outer Second Quadrant

Yan Sun^{1,2,3}, Ye Xu¹, Ji Yang¹, Fa Cheng Li¹, Xin Yu Du¹, Shao Bo Zhang¹, Xin Zhou¹

ABSTRACT

Combining HI data from the Canadian Galactic Plane Survey (CGPS) and CO data from the Milky Way Imaging Scroll Painting (MWISP) project, we have identified a new segment of a spiral arm between Galactocentric radii of 15 and 19 kpc that apparently lies beyond the Outer Arm in the second Galactic quadrant. Over most of its length, the arm is 400-600 pc thick in z . The new arm appears to be the extension of the distant arm recently discovered by Dame & Thaddeus (2011) as well as the Scutum–Centaurus Arm into the outer second quadrant. Our current survey identified a total of 72 molecular clouds with masses on the order of 10^2 - $10^4 M_{\odot}$ that probably lie in the new arm. When all of the available data from the CO molecular clouds are fit, the best–fitting spiral model gives a pitch angle of $9.3^{\circ} \pm 0.7^{\circ}$.

Subject headings: Galaxy: structure – ISM: molecules – radio lines: ISM

1. Introduction

Our knowledge of the outer Galaxy to date is largely dependent on HI emission surveys. The 21–cm line observations outline a spiral structure out to at least 25 kpc, implying a minimum radius for the gas disk (Levine et al. 2006). Through the International Galactic Plane Survey (IGPS), a widespread presence of cool HI (traced by HI absorption) was found between Galactocentric radii of 12 and 25 kpc (Strasser et al. 2007). It was not until 2011, however, that a segment of a spiral arm at radii of ~ 15 kpc was identified by Dame & Thaddeus (2011) beyond the Outer Arm in the first Galactic quadrant. This was accomplished by using the Leiden/Argentine/Bonn (LAB) 21–cm survey (Kalberla et al. 2005),

¹Purple Mountain Observatory, Chinese Academy of Sciences, Nanjing 210008, China; yansun@pmo.ac.cn

²Graduate University of the Chinese Academy of Sciences, 19A Yuquan Road, Shijingshan District, Beijing 100049, China

³Key Laboratory of Radio Astronomy, Chinese Academy of Sciences, China

and new CO observations with the 1.2 m telescope at the Harvard-Smithsonian Center for Astrophysics (CfA).

Because of the far distances involved, high-sensitivity CO observations are essential for delineating spiral structures in the extreme outer Galaxy. Digel et al. (1994) were the first to detect molecular clouds in this region. Due to the relatively low sensitivity of the Five College Radio Astronomy Observatory (FCRAO) CO survey (Heyer et al. 1998), only a few bright molecular clouds were identified there (Kerton & Brunt 2003). Until now, no coherent, large-scale structures beyond the Outer Arm have been identified in the second quadrant.

We have carried out large-scale CO mapping in the second quadrant of the Galactic plane, which is part of the Milky Way Imaging Scroll Painting (MWISP) Project¹. One of the goals of this project is to probe the spiral structures further than the Outer Arm. This mapping has completely covered the regions between $120^\circ \leq l \leq 144^\circ$ and $-2.25^\circ \leq b \leq 3.75^\circ$, and between $144^\circ \leq l \leq 150^\circ$ and $-3.75^\circ \leq b \leq 3.75^\circ$. In the longitude range of 100° to 120° , the observations so far were guided by the latitude distribution of extreme outer molecular clouds previously reported by Brunt et al. (2003) and Kerton & Brunt (2003), rather than an unbiased survey.

2. CO observations and Archival Data of atomic hydrogen

2.1. CO observations

The observations were conducted during 2011 and 2014 using the 13.7-m telescope of the Purple Mountain Observatory (PMO) in Delingha, China. The receiver was the newly installed Superconducting Spectroscopic Array Receiver (SSAR; Shan et al. 2012). All observations were carried out in “on-the-fly” (OTF) mode. The ^{12}CO , ^{13}CO and C^{18}O lines were observed simultaneously.

At 115 GHz, the main beam width was about $52''$, and the main beam efficiencies (η_{mb}) were 0.46 for ^{12}CO and 0.43 for ^{13}CO and C^{18}O . The typical rms noise level was ~ 0.5 K for ^{12}CO and 0.3 K for ^{13}CO and C^{18}O , corresponding to a channel width of 0.16 km s^{-1} . All of the spectral data were processed using the GILDAS package. It should be noted that any results presented in the figures and tables are on the brightness temperature scale (T_R^*), corrected for beam efficiencies using $T_{mb} = T_A^* / \eta_{mb}$. Details on the observations, data collection,

¹ <http://www.radioast.nsd.c.cn/yhhjindex.php>

and data processing steps will be presented in Sun et al. (2014, in prep.).

2.2. Archival Data of atomic hydrogen

The 21-cm line data were retrieved from the Canadian Galactic Plane Survey (CGPS; Taylor et al. 2003), covering Galactic longitudes from $l = 63^\circ$ to 175° and latitudes from $b = -3.5^\circ$ to $+5.5^\circ$, and a latitude extension to $b = +17.5^\circ$ between $l = 100^\circ$ to 116.5° . The velocity coverage of the data is in the range of -153 to 40 km s^{-1} with a channel separation of 0.82 km s^{-1} . The survey has a spatial resolution of $58''$ which is comparable to our CO observations.

3. Results and Discussion

We created $b - v$ maps of the HI emission in the CGPS ($66^\circ < l < 150^\circ$) and the CO emission in the MWISP ($100^\circ < l < 150^\circ$), by obtaining average emissions over a 5° wide window in longitude. The data of the CGPS in the range of $150^\circ < l < 175^\circ$ were excluded from this analysis because of the degeneracy of the radial velocity. The Outer Arm has been widely accepted as the outermost arm in the second quadrant (Russeil 2003; Russeil et al. 2007). However, all $b - v$ maps reveal a clear and distinct feature distributed beyond the Outer Arm at a maximum negative velocity. This outermost feature varies in latitude and velocity. In Figure 1, we show one of these $b - v$ distributions from both the CO (image) and the HI (contours) emissions in longitude from 127° to 132° . The Outer Arm and the outermost feature are clearly seen as strong, separate features.

To highlight the outermost feature, a $l - v$ map of integrated HI emission over a window that follows the feature in latitude is shown in Figure 2a. The high-mass star forming regions (HMSFRs) assigned to the Outer and Perseus Arms are marked with squares and diamonds, respectively (Reid et al. 2014). Similarly, Figure 2b focuses on the outermost feature, obtained by integrating the HI emission over a window that follows the feature in velocity. It is worth noting that at large negative velocities, the HI emission forms an arc from $l \sim 75^\circ$, $b \sim 3^\circ$, $v \sim -110 \text{ km s}^{-1}$, through $l \sim 110^\circ$, $b \sim 3.5^\circ$, $v \sim -105 \text{ km s}^{-1}$, to $l \sim 150^\circ$, $b \sim -2^\circ$, $v \sim -70 \text{ km s}^{-1}$, running roughly parallel to the locus of the Outer Arm but shifted by $20\text{-}30 \text{ km s}^{-1}$ to more negative velocities. This suggests that it may be a segment of a major spiral arm since spiral arms have long been recognized as presenting coherent arcs and loops in Galactic $l - v$ plots of atomic and molecular emissions (Weaver 1974; Dame et al. 1986; Dame & Thaddeus 2008, 2011). The present feature was largely overlooked

in the past since only short segments of it appear in l-v diagrams at any specific latitude or even in an l-v diagram integrated over all latitudes covered by the CGPS (e.g., in Figure 3 of Strasser et al. 2007).

Before giving an explicit claim of a new spiral arm, we investigated the characteristics of the outermost feature in more detail. So far a total of 72 molecular clouds that are probably attributed to the outermost feature were detected by MWISP. These 72 clouds are marked with circles in Figures 2 and 3 and also summarized in Table 1. More than 10 clouds show clear ^{13}CO detections while many of other clouds were only marginally detected. However, none of them show C^{18}O detections. The isotope abundance ratios in the extreme outer Galaxy will be studied in the forthcoming deep observations. Actually, all known clouds in the extreme outer Galaxy reported by Digel et al. (1994) and Kerton & Brunt (2003) were detected by the present survey. We labelled all these known clouds in column (1) of Table 1. Note that the clouds reported by Digel et al. (1994) in the higher longitude range of $145^\circ < l < 151^\circ$ are not included in Table 1, since these clouds are partially blended in velocity with emission at less negative velocities. Besides, they might lie in the Outer arm or in the inter-arm on the assumption of the rotation curve of Reid et al. (2014).

Most of the clouds are newly discovered, which suggests that we may still miss some molecular clouds in the interval $100^\circ < l < 120^\circ$ due to the narrow latitude coverage. The derived masses, mainly on the order of $10^3 M_\odot$ to $10^4 M_\odot$, fall in the typical range for the masses of molecular clouds that are usually confined to spiral arms. Note that the mass is a lower limit, since the adopted CO-to- H_2 X factor $1.8 \times 10^{20} \text{ cm}^{-2}$ is measured in the solar neighborhood. However, a recent study suggested that the X factor rises by a factor of 2–3 between the solar circle and the circle at $R_{\text{Gal}}=14 \text{ kpc}$ (Abdo et al. 2010). In addition, the beam dilution effects lower the signal-to-noise ratio and hence also reduce the derived masses. We have selected one example with the largest negative velocities we recently detected (molecular cloud 24 marked with cross) and presented the velocity-integrated intensity and spectrum of the peak emission in Figure 2b. Although these molecular clouds are more sparsely distributed than the atomic gas, both explicitly trace the same coherent, large-scale structure, i.e., the new arm well.

The warp of the Galactic disk is obvious (Figure 2b), which exhibits a clear positive warp between $l = 66^\circ$ and 135° , and a negative warp between $l = 135^\circ$ to 150° . Assuming a mean distance of 12 Kpc, the new arm with thickness in z of about 2° to 3° correspond to about 400 to 600 pc. Generally, the new arm is more severely warped and thicker than the Outer Arm. This is in good agreement with the theory for both external spiral galaxies and our Galaxy, which suggests that the warping and thicknesses of the disks increase with increasing distance from the galactic center (Wouterloot et al. 1990; Russeil 2003; Bottema

1996). Moreover, the new arm is distinct from the Outer Arm with a spatial separation of about 3–4 kpc, which is consistent with the typical span of the spiral arms outside the Perseus Arm (Reid et al. 2014; Vallée 2014).

Locations of all available molecular clouds in the far outer Galaxy are compared with the spiral arm model in Figure 3, superposed on: (a) CO $l-v$ diagram from Dame et al. (2001), and (b) an artist’s conception of the Milky Way (R. Hurt: NASA/JPL-Caltech/SSC). The artist’s image has been scaled to place the HMSFRs in the spiral arms. These clouds are indicated by filled stars, triangles and circles, which cover Galactic longitudes from $l=13^\circ$ to 55° detected by Dame & Thaddeus (2011), and from $l=100^\circ$ to 150° detected by us. The squares indicate the locations of the HMSFRs associated with the Outer Arm (Reid et al. 2014). The white dashed line in Figure 3 is a log spiral that was fit to the Scutum-Centaurus arm in the inner Galaxy (Vallée 2008, 2014). Generally, our data are in agreement with the far-extension of the Scutum-Centaurus Arm in the second quadrant. However, confirmation of this hypothesis would be a challenge as suggested by Dame & Thaddeus (2011).

We attempted to fit the distribution of these outermost clouds, adopting a log–periodic spiral model defined by $\ln(R/R_{\text{ref}}) = -(\beta - \beta_{\text{ref}})\tan\psi$, where R is the Galactocentric radius at a Galactocentric azimuth β for an arm with a radius R_{ref} at reference azimuth β_{ref} and pitch angle ψ . The Bayesian Markov chain Monte Carlo (MCMC) procedure was adopted to estimate the parameters R_{ref} and ψ (see paper of Reid et al. (2014) for more details). The best–fitting spiral model for the CO data on the interval $120^\circ \leq l \leq 150^\circ$ is $R_{\text{ref}} = 17.8 \pm 1.0$ kpc at $\beta_{\text{ref}} = 27.0^\circ$ and $\psi = 10.8^\circ \pm 7.6^\circ$ (indicated by the red dashed line in Figure 3). The best–fitting spiral model for all of the available CO data including clouds detected by Dame & Thaddeus (2011) is $R_{\text{ref}} = 16.1 \pm 1.0$ kpc at $\beta_{\text{ref}} = 43.9^\circ$ and $\psi = 9.3^\circ \pm 0.7^\circ$ (indicated by the cyan solid line in Figure 3). The uncertainties give a 68% confidence range.

The consistent fitting results confirm that the new arm can be interpreted as the far-extension of the distant arm recently discovered by Dame & Thaddeus (2011). Apparently, both models fit the data well over a wide longitude range, except in $l=100^\circ$ to 116° , where the model deviates from the data. Such departures might be caused by the kinematic distance uncertainty. Indeed, any systematic velocity departures can lead to distance uncertainty. The velocity departures, including both positive and negative values have already been observed, e.g., in the Perseus Arm between 90° and 150° and the Sagittarius-Carina Arm (Russeil 2003). Another possibility is the bias introduced by the incompleteness of the sample due to the narrow latitude coverage in this longitude interval, as mentioned above. The parallax measurements and MWISP projects in progress will be required to solve the problem and determine the new arm more accurately.

We are grateful to all of the staff of the 14-m telescope of the PMO for their dedicated assistance. We would like to thank Dr. Mark Reid for using of his fitting procedure. We thank Dr. Yuan-Wei Wu for his useful discussions. We also thank the anonymous referee for very helpful suggestions and comments that help improved the paper. Research for this project is supported by the National Natural Science Foundation of China (grant Nos. 11003046, 11233007, 11133008, 11403104), the Strategic Priority Research Program of the Chinese Academy of Sciences (grant No. XDB09000000), and the Key Laboratory for Radio Astronomy, CAS.

REFERENCES

- Abdo, A. A. et al. 2010, *ApJ*, 710, 133
- Brand, J., & Wouterloot, J. G. A. 1994, *A&AS*, 103, 503
- Bottema, R. 1996, *A&A*, 306, 345
- Brunt, C. M., Kerton, C. R., Pomerleau, C. ., & Thaddeus, P. 1985, *ApJ*, 297, 751
- Dame, T. M., Elmegreen, B. G., Cohen, R. S., & Thaddeus, P. 1986, *ApJ*, 305, 892
- Dame, T. M. et al. 1987, *ApJ*, 322, 706
- Dame, T. M., Hartmann, D., Thaddeus, P. 2001, *ApJ*, 547, 792
- Dame, T. M., & Thaddeus, P. 2008, *ApJ*, 683L, 143
- Dame, T. M., & Thaddeus, P. 2011, *ApJ*, 734L, 24
- Digel, S., de Geus, E., & Thaddeus, P. 1994, *ApJ*, 422, 92
- Heyer, M. H., Brunt, C., Snell, R. L., Howe, J. E., Schloerb, F. P., & Carpenter, J. M. 1998, *ApJS*, 115, 241
- Kalberla, P. M. W., Burton, W. B., Hartmann, D., Arnal, E. M., Bajaja, E., Morras, R., Poppel, W. G. L. 2005, *A&A*, 440, 775
- Kerton, C. R., & Brunt, C. M. 2003, *A&A*, 399, 1083
- Levine, E. S., Blitz, L., Heiles, C. 2006, *Science*, 312, 1773
- Reid, M. J. et al. 2014, *ApJ*, 783, 130

- Russeil, D., 2003, *A&A*, 397, 133
- Russeil, D., Adami, C., Georgelin, Y. M., 2007, *A&A*, 470, 161
- Shan, W., Yang, J., Shi, S., et al. 2012, *IEEE Trans. Terahertz Sci. Technol.*, 2, 593
- Strasser, S. T. et al. 2007, *AJ*, 134, 2252
- Sun et al. 2014, in prep.
- Taylor et al. 2003, *AJ*, 125, 3145
- Weaver, H. 1974, *IAUS*, 60, 573
- Wouterloot, J. G. A., Brand, J., Burton, W. B., Kwee, K. K., 1990, *A&A*, 230, 21
- Vallée, J. P., 2008, *AJ*, 135, 1301
- Vallée, J. P., 2014, *AJ*, 148, 5

Table 1. Parameters of molecular clouds derived by CO(1-0).

Number	l	b	V_{lsr}	T_{peak}	ΔV	W_{CO}	area	d	R	Z scale	radius	Mass
(1)	($^{\circ}$)	($^{\circ}$)	(km s^{-1})	(K)	(km s^{-1})	(K.km s^{-1})	(arcmin^2)	(kpc)	(kpc)	(kpc)	(pc)	($10^3 M_{\odot}$)
	(2)	(3)	(4)	(5)	(6)	(7)	(8)	(9)	(10)	(11)	(12)	(13)
1	101.992	3.016	-101.0	3.0	3.3	10.4	39.4	9.8	14.2	0.5	10.1	13.0
2	102.092	2.776	-102.9	3.5	2.4	8.9	13.4	10.1	14.4	0.5	5.9	3.9
3	102.375	2.733	-102.6	4.6	1.3	6.2	29.0	10.0	14.4	0.5	8.8	5.9
4	103.042	2.475	-106.4	2.5	1.2	3.3	3.2	10.5	14.8	0.5	2.8	0.3
5	103.458	3.300	-108.1	3.0	0.9	2.8	3.7	10.7	15.0	0.6	3.1	0.3
6	103.729	2.867	-100.5	3.2	1.8	6.1	6.5	9.7	14.2	0.5	3.9	1.1
7*	104.983	3.317	-102.7	5.8	1.9	11.4	36.2	9.9	14.5	0.6	9.7	13.1
8*	105.242	3.025	-100.9	4.0	1.7	7.5	37.5	9.6	14.3	0.5	9.6	8.5
9	105.283	3.175	-106.5	3.9	2.0	8.1	5.6	10.4	15.0	0.6	3.8	1.5
10	106.417	3.925	-112.0	1.5	1.1	3.2	18.3	11.1	15.7	0.8	7.6	2.3
11*	107.725	2.933	-102.1	2.5	1.8	4.8	27.5	9.7	14.6	0.5	8.2	4.0
12	107.900	1.908	-102.5	1.8	2.4	4.5	10.9	9.7	14.7	0.3	5.1	1.5
13	109.200	2.283	-103.0	4.3	0.7	3.4	5.9	9.8	14.8	0.4	3.7	0.6
14*	109.292	2.083	-101.2	5.2	2.1	11.5	22.1	9.5	14.6	0.3	7.3	7.5
15*	109.375	2.642	-98.6	3.6	1.5	5.9	11.9	9.2	14.3	0.4	5.1	1.9
16*	109.500	2.608	-99.6	4.5	1.5	7.4	55.8	9.3	14.5	0.4	11.3	11.7
17*	109.642	2.700	-98.8	4.8	1.8	9.1	40.8	9.2	14.4	0.4	9.6	10.3
18*	109.790	2.717	-99.2	5.8	1.7	10.3	21.9	9.2	14.4	0.4	7.0	6.2
19	110.025	3.083	-98.1	3.3	0.8	2.9	22.5	9.1	14.3	0.5	7.0	1.7
20	110.167	2.783	-98.3	3.2	1.0	3.3	8.1	9.1	14.4	0.4	4.1	0.7
21*	114.342	0.781	-100.9	7.9	2.1	18.0	113.7	9.5	15.0	0.1	16.5	60.5
22	115.992	1.250	-115.8	2.4	1.1	2.6	6.2	11.9	17.3	0.3	4.7	0.7
23*	116.725	3.542	-107.6	5.5	1.9	11.3	22.8	10.5	16.1	0.6	8.1	9.2
24	117.367	1.700	-120.8	2.1	2.3	5.1	83.7	13.0	18.4	0.4	19.5	23.8
25*	117.576	3.950	-106.0	5.9	1.2	7.7	18.7	10.3	16.0	0.7	7.2	4.9
26*	118.143	3.417	-106.7	2.8	1.6	4.9	18.1	10.4	16.2	0.6	7.2	3.1
27	120.925	2.758	-103.3	2.8	1.6	4.8	6.3	10.1	16.1	0.5	4.0	0.9
28	121.375	2.708	-103.6	2.3	0.9	2.4	22.2	10.2	16.2	0.5	7.8	1.8
29*	121.675	2.042	-101.5	2.6	1.4	3.9	32.7	9.9	16.0	0.4	9.2	4.1
30*	121.817	3.052	-103.9	5.6	2.3	13.7	78.7	10.3	16.4	0.5	14.9	37.6
31	121.967	1.842	-102.8	2.5	1.1	3.0	25.9	10.1	16.2	0.3	8.4	2.6
32*	122.375	1.775	-102.5	3.0	1.2	3.9	70.0	10.1	16.3	0.3	13.9	9.2
33	122.492	2.592	-105.1	2.4	1.4	3.5	31.5	10.6	16.7	0.5	9.7	4.0
34*	122.775	2.522	-107.2	5.5	2.2	12.8	91.8	11.0	17.1	0.5	17.3	47.0
35*	123.367	1.659	-103.2	2.6	2.3	6.5	66.0	10.4	16.5	0.3	13.8	15.2
36	123.650	2.833	-104.9	3.1	1.1	3.6	35.5	10.7	16.9	0.5	10.4	4.8
37	123.925	3.158	-105.4	2.9	1.1	3.2	13.6	10.8	17.0	0.6	6.4	1.6
38	124.292	3.000	-109.8	1.9	1.8	3.6	15.1	11.7	17.9	0.6	7.4	2.4
39	124.342	3.367	-104.9	1.8	1.4	2.8	8.7	10.8	17.0	0.6	5.1	0.9
40	124.525	3.400	-103.9	2.7	0.8	2.3	15.3	10.6	16.8	0.6	6.7	1.3
41	125.075	2.375	-106.9	1.7	2.1	3.9	41.4	11.3	17.5	0.5	11.9	6.8
42	127.150	2.583	-101.5	2.1	1.4	3.1	35.0	10.6	17.0	0.5	10.2	4.0
43*	127.875	2.167	-99.6	2.4	2.0	4.9	81.0	10.4	16.9	0.4	15.3	14.1
44	128.633	2.833	-102.4	2.2	0.9	2.2	8.0	11.1	17.6	0.5	5.0	0.7
45	130.050	2.108	-102.5	3.6	0.9	3.4	18.6	11.4	18.0	0.4	8.0	2.7
46†	131.016	1.524	-102.2	2.5	2.7	7.2	33.8	11.6	18.3	0.3	11.0	10.8
47†*	131.157	1.390	-100.6	3.8	2.2	8.6	15.9	11.3	18.0	0.3	7.3	5.6
48	131.575	1.300	-104.5	1.9	0.8	1.6	6.1	12.4	19.0	0.3	4.8	0.5
49	132.792	-0.425	-97.1	1.8	2.1	3.9	10.2	11.0	17.8	-0.1	5.6	1.5
50	133.817	-0.758	-94.7	4.6	1.1	5.4	31.3	10.7	17.6	-0.1	9.8	6.3
51	133.825	-0.017	-91.2	1.7	1.0	1.8	3.0	10.0	16.9	-0.0	2.6	0.2
52	136.859	1.557	-90.6	2.3	1.5	3.5	16.3	10.7	17.8	0.3	7.0	2.1
53*	137.283	-1.150	-101.6	2.7	2.4	6.9	13.2	14.0	20.9	-0.3	8.2	5.7
54	137.517	-1.267	-98.4	1.7	1.8	3.2	10.5	13.1	20.1	-0.3	6.8	1.8
55	137.617	-1.225	-98.7	3.4	1.5	5.6	10.6	13.2	20.2	-0.3	6.9	3.3
56†*	137.759	-0.983	-103.0	5.9	2.8	17.6	41.0	14.7	21.7	-0.3	15.4	51.4
57†*	137.775	-1.067	-102.1	5.0	2.3	12.2	43.0	14.4	21.4	-0.3	15.4	35.9
58	138.373	-0.850	-94.4	1.9	1.6	3.2	8.7	12.3	19.4	-0.2	5.8	1.3
59	139.116	-1.475	-96.8	4.9	1.3	6.7	4.6	13.4	20.5	-0.3	4.4	1.6
60	139.850	0.368	-88.9	1.9	1.4	2.9	5.2	11.4	18.6	0.1	4.0	0.6
61	140.183	0.258	-88.3	2.0	0.8	1.8	8.1	11.4	18.6	0.1	5.1	0.6
62	140.700	0.150	-86.9	1.9	1.2	2.5	8.0	11.2	18.5	0.0	5.0	0.8
63	141.083	0.425	-85.0	1.3	1.9	2.6	8.3	10.8	18.2	0.1	5.0	0.8
64	142.167	0.267	-85.8	1.6	1.3	2.3	9.5	11.6	18.9	0.1	5.7	0.9
65†	142.642	0.317	-81.1	2.0	1.0	2.0	49.0	10.5	17.9	0.1	12.0	3.5

Table 1—Continued

Number	l	b	V_{lsr}	T_{peak}	ΔV	W_{CO}	area	d	R	Z scale	radius	Mass
(1)	($^{\circ}$)	($^{\circ}$)	(km s^{-1})	(K)	(km s^{-1})	(K.km s^{-1})	(arcmin^2)	(kpc)	(kpc)	(kpc)	(pc)	($10^3 M_{\odot}$)
(1)	(2)	(3)	(4)	(5)	(6)	(7)	(8)	(9)	(10)	(11)	(12)	(13)
66	143.325	1.775	-79.9	2.7	1.1	3.1	17.9	10.4	17.9	0.3	7.1	1.9
67	143.533	0.492	-76.7	4.0	1.6	6.5	12.8	9.7	17.2	0.1	5.6	2.5
68	144.167	0.817	-74.6	3.0	1.4	4.6	6.3	9.4	16.9	0.1	3.7	0.8
69	145.208	-0.392	-74.0	4.8	1.7	8.8	7.5	9.7	17.2	-0.1	4.2	1.9
70	145.808	-1.817	-79.6	1.8	1.8	3.6	17.1	11.6	19.2	-0.4	7.8	2.7
71	145.850	-1.717	-78.6	2.5	1.7	4.4	60.0	11.3	18.9	-0.3	14.3	11.2
72	146.059	-1.650	-77.2	4.9	1.7	8.7	17.6	11.0	18.6	-0.3	7.5	6.0

Note. — Column (1): source number which is organized by increasing galactic longitude. Sources detected by Digel et al. (1994) and Kerton & Brunt (2003) are marked with † and *. Columns (2)-(3): Galactic coordinates of the CO emission peak. Columns (4)-(7): results of Gaussian fit to the spectra. Column (8): angular area of the complex defined by the 3σ limits. Columns (9)-(10): the heliocentric distance d , and the Galactocentric distance R , respectively; both are derived from the rotation curve of Reid et al. (2014), assuming $R_{\odot} = 8.34$ kpc and $\Theta_0 = 240$ km s^{-1} . Column (11): scale height, z , $z = D \sin(b)$. Column (12): equivalent radii of the molecular clouds corrected by the beam size of the telescope. Column (13): cloud mass calculated using $X = 1.8 \times 10^{20}$ (Dame et al. 2001).

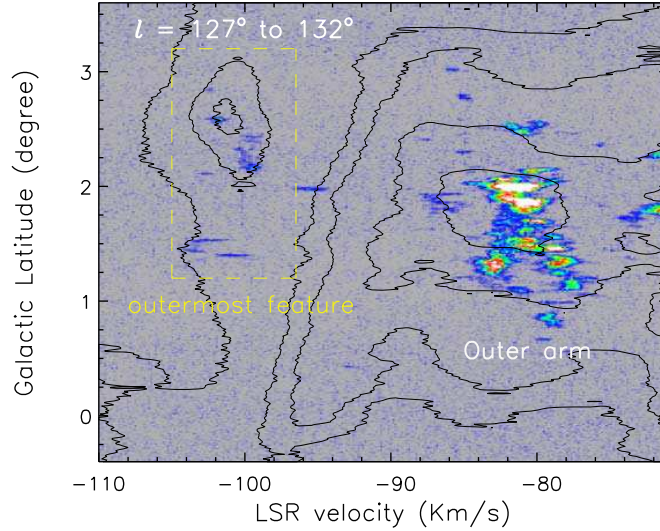


Fig. 1.— Latitude–velocity diagrams of CO (image) and HI (contours) integrated in l from 127° to 132° . The dashed box indicates the approximate boundaries of the outermost feature. The contour levels are 35, 75, 100, 150 and 200 K. The Outer Arm and the outermost feature are clearly seen as strong, separate features.

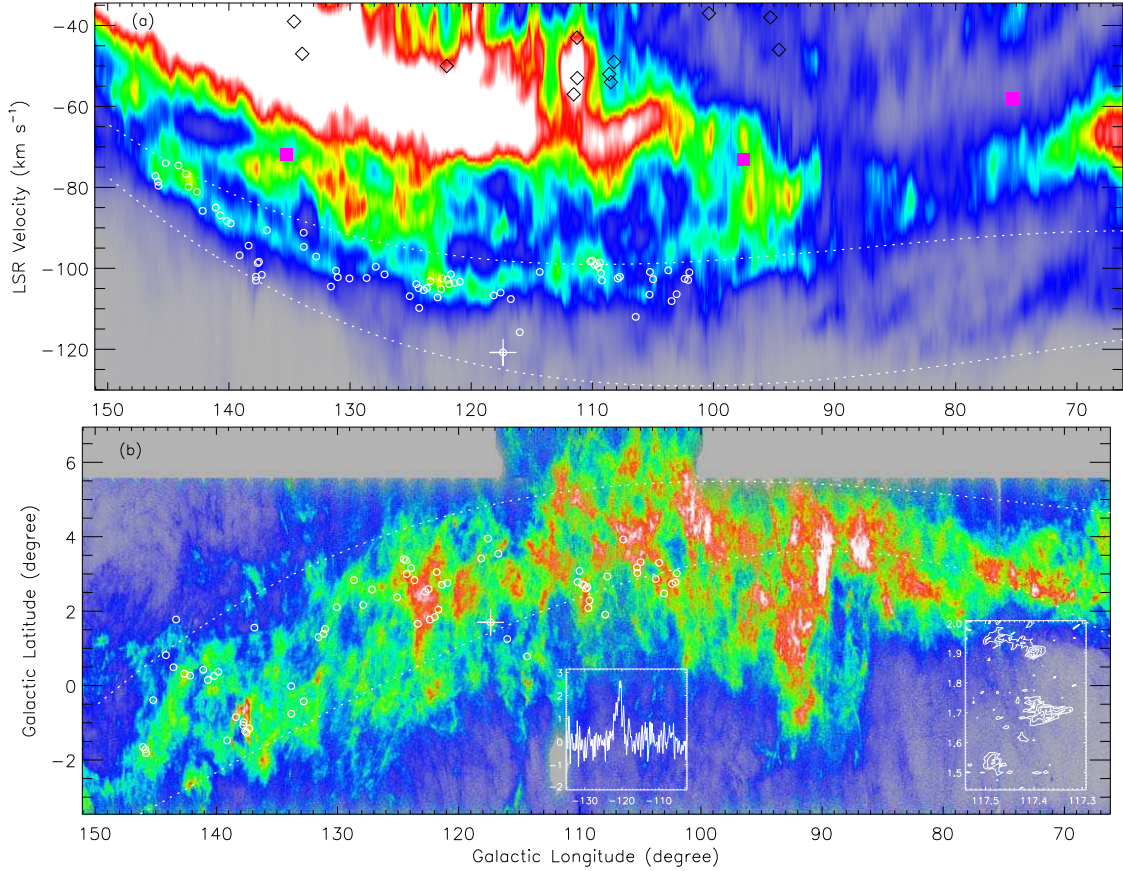


Fig. 2.— (a) Longitude-velocity diagram of HI (image), integrated over a window that follows the new arm in latitude. The circles mark the locations of the molecular complexes summarized in Table 1. The HMSFRs assigned to the Outer and Perseus arms are marked with squares and diamonds (Reid et al. 2014). (b) Velocity integrated intensity of HI corresponding to the new arm. The integrated velocity window is marked by the two dashed lines in the upper panel. The insets show the velocity-integrated CO map and spectrum of peak emission of molecular clouds 24 (marked with cross). The lowest contour level is 3σ .

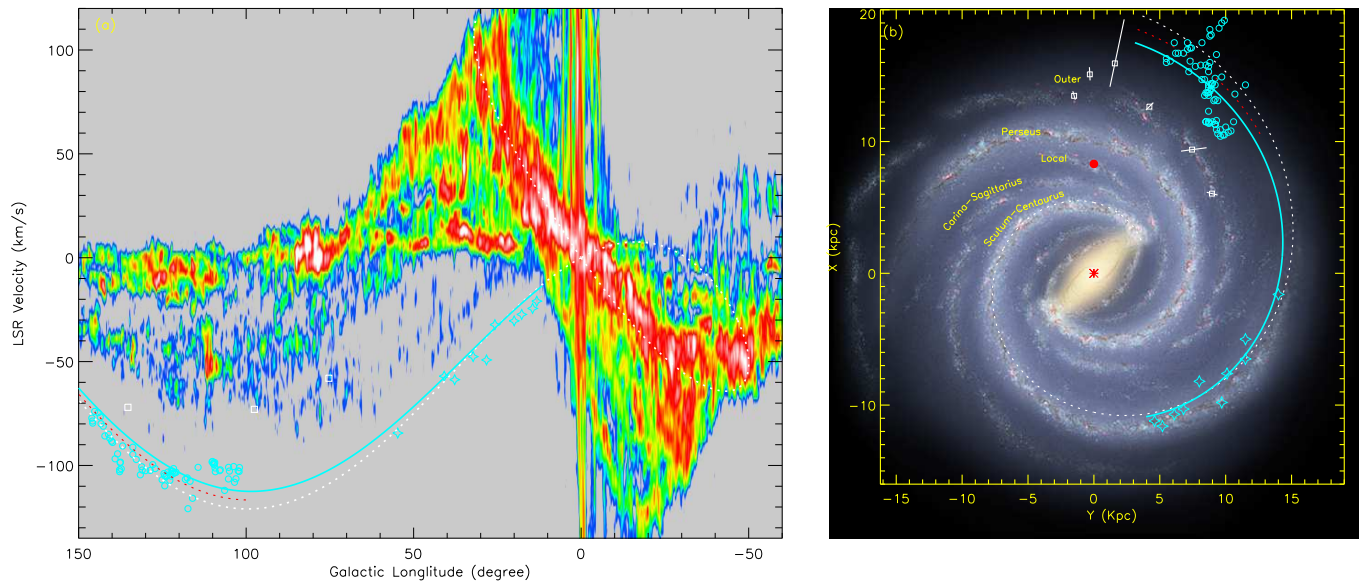


Fig. 3.— Locations of molecular clouds in the far outer Galaxy superposed on: (a) CO longitude velocity diagram from Dame et al. (2001), and (b) an artist’s conception of the Milky Way (R. Hurt: NASA/JPL-Caltech/SSC). The filled stars and circles mark clouds covering Galactic longitudes from $l=13^\circ$ to 55° detected by Dame & Thaddeus (2011), and $l=100^\circ$ to 150° detected by us, respectively. The squares indicate the locations of HMSFRs associated with the Outer arm. The white dashed line is a log spiral with a mean pitch angle of 12° that was fit to the Scutum-Centaurus arm in the inner Galaxy (Vallée 2008, 2014). The red dashed line traces the log-periodic spiral fitting results to data in 120° to 150° , while the cyan solid line traces the fitting results to all available data including clouds detected by Dame & Thaddeus (2011) (see Section 3).